Supporting Information

Microfluidic membraneless microbial fuel cells: New protocols for record power

densities

Nastaran Khodaparastasgarabad[1], Jayesh M. Sonawane[1], Haleh Baghernavehsi,[1] Lingling Gong[1],

Linlin Liu,[1] Jesse Greener[1,2]*

[1] Département de Chimie, Faculté des sciences et de génie,

Université Laval, Québec City, QC, Canada

[2] CHU de Québec, Centre de recherche,

Université Laval, 10 rue de l'Espinay, Québec, QC, Canada

* Corresponding author: jesse.greener@chm.ulaval.ca

Table of contents:

Section S1: Effect of pressure drop channels

In this study, we implemented certain design features in microfluidic microbial fuel cells to improve their performance. One of these features was pressure-drop channels, which decouples the pressure pulses between their upstream sources (stick-slip in pumps and syringes) and the on-chip electrochemical cell. The other feature was a system for continuous, bubble-free liquid delivery, which was implemented using four-way valves that enabled flow calming and de-bubbling before introduction to the chip. In the Supporting Figure 1, we showcase the effect of these two features via potential versus time growth curves that were collected after inoculation. Compared to the growth curve for the MFC in which the design improvements were not implemented, the data were smoother and generally showed a higher output. For example, in the microfluidic MFC that did not implement the two flow improvements, the growth curve in times day 0 to day 1 shows more "noise", which is actually complex frequency oscillations in the voltage (with frequency components ranging from approximately 15 minutes to 2 hours). These oscillations are less obvious in the rapid growth region after day two, but some effect is visible throughout the experiment and especially after the growth rate becomes reduced after four days. As seen in Figure S1, the oscillations can often be worse immediately following a syringe replacement if no four-way valves are used. These oscillations occur because bubbles entering the MFC complicate the flow and pressure profiles due to their growth through the flow into the device, subsequent nucleation, merging, and eventual disappearance through detachment and dissolution.
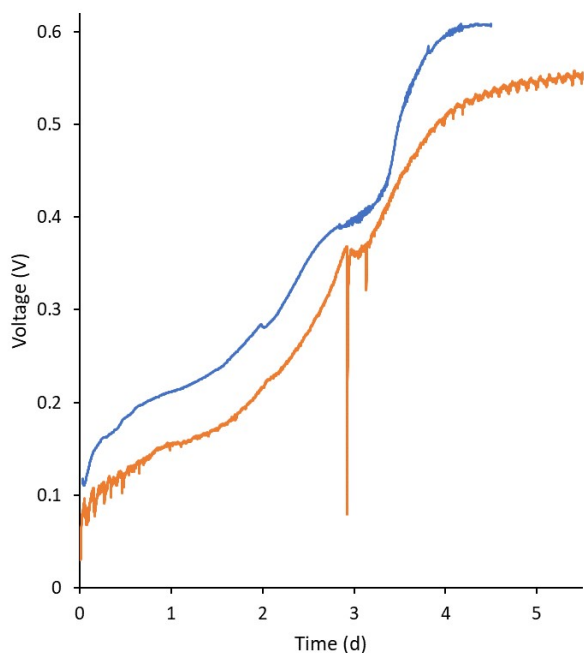
Figure S1. Voltage versus time profile for a microfluidic MFC with (blue) and without (orange) pressure-drop channels and continuous, bubble-free liquid delivery using four-way valves. The flow rate was Q_T=1 mL h^{-1} using a co-flow of acetate nutrient solution (10 mM) and ferricyanide (30 mM).

Section S2: Simulations based on electroactive biofilm (EAB) patterns after approximately one week

(a) Details of the 3D model

The model consisted of an anode channel with an electron collector (anode electrode), and an electron collector (cathode electrode). An electroactive biofilm (EAB) was placed on the anode. The EAB had a height 60 μm in the locations shown in Figure S2a/b for the 10 mm width anode device (Figure S2a) and the 3 mm anode device (Figure S2b), called the modified and unmodified MFCs, respectively. The biofilm patterns are based on those which are shown in Figures 3a(i) and 3a(ii), respectively. We also assumed no slip conditions applied at all walls, including along the EAB liquid/surface interface. See previous studies where parameters are defined.[1,2] We assumed that all species were "dilute", that is, that their concentrations were less than 10 mol% of the solvent fluid, and as such mixture properties such as density and viscosity are assumed to correspond to those of the solvent. This was implemented by the use of COMSOL's physics for "Transport of Diluted Species" which accounted for conservation equations for mass transport and

3

for mass transport by diffusion and advection as well as migration in an electric field. In the electrolyte flow channel, the transport of each species was governed by the Nernst equation. Nernst equation was also applied in the electrode zone. The initial value of electrode current density was applied the same as the maximum value observed in Figure 2 in the main paper (approximately 1 and 2 A m^{-2}) to decrease the time of calculation. A secondary current distribution was applied in which the effect of the electrode kinetics in addition to solution resistance are accounts for. The assumptions about the electrolyte composition and behavior came from Butler Volmer equation

(a)

(b)
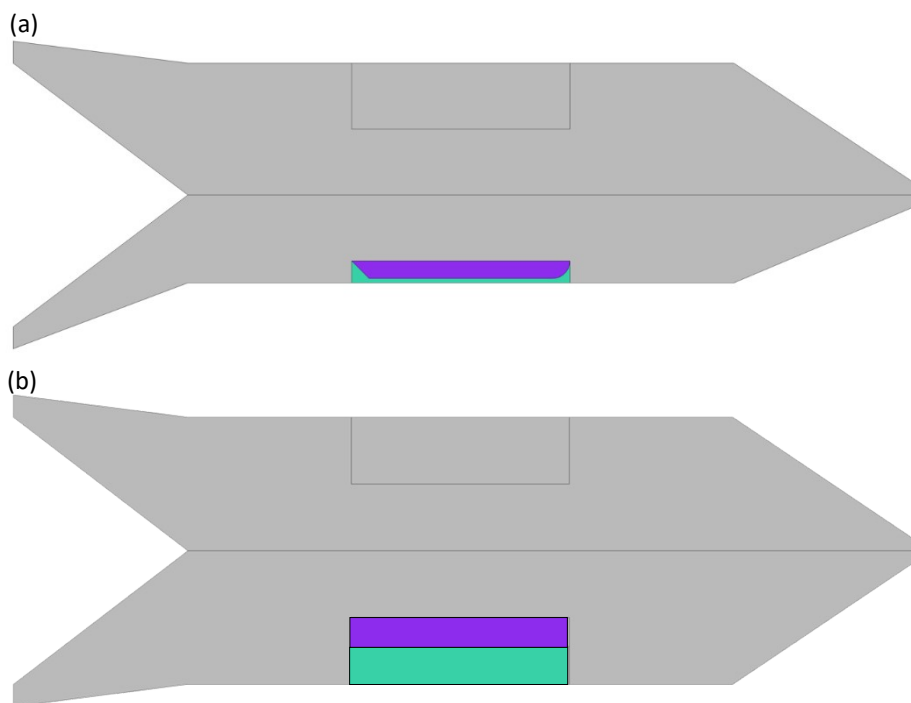
and concentration dependent kinetics, which resulting in Ohm's law for electrolyte current.

Figure S2. Geometrical model for fluidic simulations showing EAB growth with the approximate patterns observed by microscopy after one week for the modified 1 mm anode device (a) and the unmodified 3 mm anode device (b). Purple shows the position of the biofilm, and green the position of the colonized electrode.

(b) Modeling results after 1

We used the model described in the previous section to model electron generation rate across the EAB surfaces from the unmodified (3 mm anode) MFC and the modified one (1 mm anode). Results are presented in Figures S3a and S3b, respectively. Acetate consumption can be obtained by dividing by 8, based on the reaction stoichemetry:

$CH_3HOO^- \rightarrow 2CO_2 + 7H^+ + 8e^-$ Eqn. S1

Generally there is a jump in results at the biofilm edge. This is likley due to a combination of local high concentration at the upstream side and mesh errors at the edges of the electrodes.
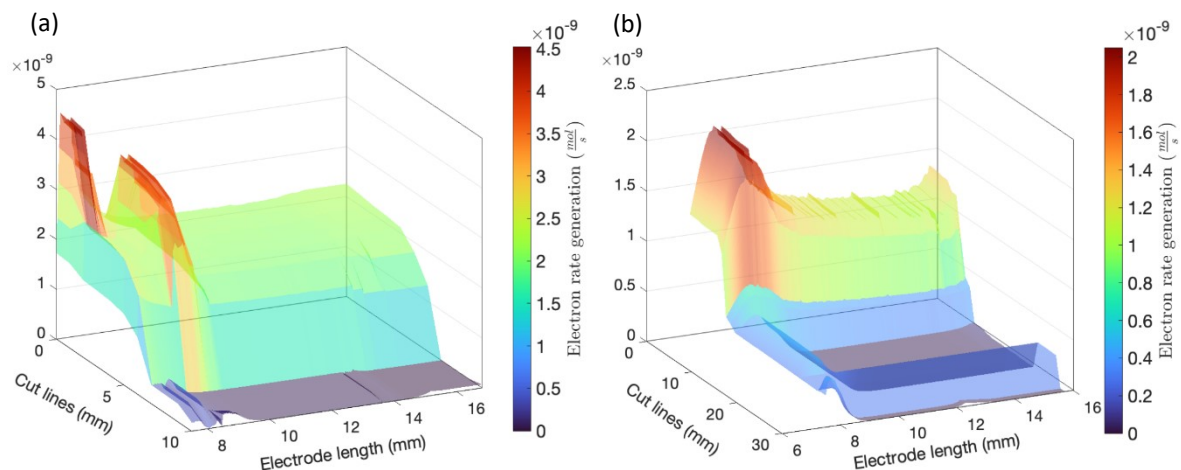

Figure S3. Simulation results for electron generation rate for the (a) unmodified (3 mm electrode) and the (b) modified (1 mm electrode) membraneless MFCs.

Section S3: Electrolyte current density and choice of normalization area $A_{electrolyte}$

It is hypothesized in this paper that there are two reasons for the traditionally low areal power densities in microfluidic MFCs. One is the difficulty in maintaining ideal culture conditions in membraneless devices due to the potential for fluid cross-over. This paper makes major advances on that part via new technological innovations as outlined in the main paper. The second is hypothesized to stem from the low ceiling in most microfluidic devices. In ours that is only 0.16 mm. This results in a highly constrained travel path for current between the electrodes, which may be as strong or stronger a limitation on the current density than projected electrode surface area. Therefore, we recommend authors report using a new approach to normalizing power and current by using the cross-section area that divides electrodes (red cut-line in Figure S3a). We modeled the current de nsity for the modified microfluidic device (with a 1 mm anode) and present results in Figure S3. In this view it can be seen that the current passes through the entire device cross-s ection (from upstream to downstream). Therefore, when mimicking the approach used in macroscale studies of normalizing by the cross-section area between the electrodes, we choose

here to use the entire cross-section area down the centre of the device. Thus, we obtained the normalization constant $A_{electrolyte}$=4.8 mm^2 (30 mm in the y-direction multiplied by 0.16 mm in the
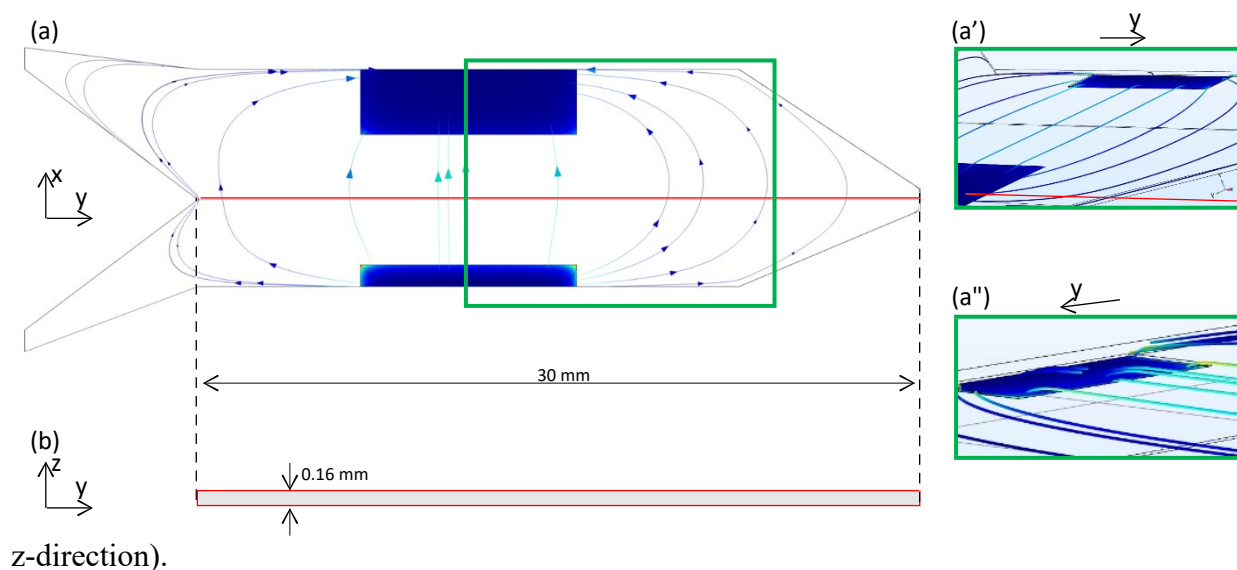

z-direction).

Figure S4. (a) A view from the x-y plane (bird's eye) that shows current density path through the electrolyte leaving the anode (bottom) arriving at the cathode (top), using the 3D geometry described above for Figure S2a. Green box shows the approximate position (a' and a"), isometric views of indicating that current flow through the electrolyte is constrained in the z-direction but not in the x- or y-directions. (b) A view from the z-y plane that shows the cross-section area that separates electrodes.

Section S4: Supplementary references

[1] L. Gong, N. Khodaparastasgarabad, D. M. Hall and J. Greener, *Electrochimica Acta*, 2022, **431**, 141071.
[2] M. A. Amirdehi, N. Khodaparastasgarabad, H. Landari, M. P. Zarabadi, A. Miled and J. Greener, *ChemElectroChem*, 2020, **7**, 2227-2235.